

**Title:** Alloxan disintegrates the plant cytoskeleton and suppresses *mlo*-mediated powdery mildew resistance

**Running head:** Alloxan suppresses *mlo*-mediated resistance

**Corresponding author:** R. Panstruga, Institute for Biology I, Unit of Plant Molecular Cell Biology, Worringerweg 1, 52056 Aachen, Germany, telephone +49 241 80 26655, fax +49 241 80 22637, e-mail [panstruga@bio1.rwth-aachen.de](mailto:panstruga@bio1.rwth-aachen.de)

**Subject areas:** Environmental and stress responses, cell-cell interactions

**Number of black and white Figures:** 0

**Number of color Figures:** 6

**Number of Tables:** 1

**Supplementary material:** 18 Figures, 5 Movies

# Alloxan disintegrates the plant cytoskeleton and suppresses *mlo*-mediated powdery mildew resistance

**Running head:** Alloxan suppresses *mlo*-mediated resistance

Hongpo Wu <sup>1</sup>, Weiwei Zhang <sup>2</sup>, Martin Schuster <sup>3</sup>, Marcin Moch <sup>4</sup>, Reinhard Windoffer <sup>4</sup>, Gero Steinberg <sup>3</sup>, Christopher J. Staiger <sup>2,5</sup>, Ralph Panstruga <sup>1,\*</sup>

<sup>1</sup> Institute for Biology I, Unit of Plant Molecular Cell Biology, Worringerweg 1, 52056 Aachen, Germany.

<sup>2</sup> Department of Biological Sciences, Purdue University, West Lafayette, Indiana 47907, USA.

<sup>3</sup> School of Biosciences, University of Exeter, Exeter EX4 4QD, UK.

<sup>4</sup> Institute of Molecular and Cellular Anatomy, RWTH Aachen University, Aachen, Germany.

<sup>5</sup> Department of Botany and Plant Pathology, Purdue University, West Lafayette, Indiana 47907, USA.

\* Corresponding author: +49 241 8026655; [panstruga@bio1.rwth-aachen.de](mailto:panstruga@bio1.rwth-aachen.de)

## ORCID:

Marcin Moch <http://orcid.org/0000-0003-2143-5292>

Ralph Panstruga <http://orcid.org/0000-0002-3756-8957>

Martin Schuster <http://orcid.org/0000-0002-6796-9196>

Christopher J. Staiger <https://orcid.org/0000-0003-2321-1671>

Weiwei Zhang <https://orcid.org/0000-0002-4754-6241>

## Abstract

Recessively inherited mutant alleles of *Mlo* genes (*mlo*) confer broad-spectrum penetration resistance to powdery mildew pathogens in angiosperm plants. Although a few components are known to be required for *mlo* resistance, the detailed molecular mechanism underlying this type of immunity remains elusive. In the present study, we identified alloxan (5,5-dihydroxyl pyrimidine-2,4,6-trione) and some of its structural analogs as chemical suppressors of *mlo*-mediated resistance in monocotyledonous barley (*Hordeum vulgare*) and dicotyledonous *Arabidopsis thaliana*. Apart from *mlo* resistance, alloxan impairs non-host resistance in *Arabidopsis*. Histological analysis unraveled that the chemical reduces callose deposition and hydrogen peroxide accumulation at attempted fungal penetration sites. Fluorescence microscopy revealed that alloxan interferes with the motility of cellular organelles (peroxisomes, endosomes and the endoplasmic reticulum) and the pathogen-triggered redistribution of the PEN1/SYP121 t-SNARE protein. These cellular deficits are likely the consequence of disassembly of actin filaments and microtubules upon alloxan treatment. Similar to the situation in animal cells, alloxan elicited the temporary accumulation of reactive oxygen species (ROS) in cotyledons and rosette leaves of *Arabidopsis* plants. Our results suggest that alloxan may destabilize cytoskeletal architecture *via* induction of an early transient ROS burst, further leading to the failure of molecular and cellular processes that are critical for plant immunity.

## Keywords

Alloxan, chemical biology, cytoskeleton, *mlo* resistance, pharmacological inhibition, powdery mildew

## Introduction

Powdery mildew is a prevalent fungal disease of angiosperm plants in temperate climates that is caused by obligate biotrophic pathogens belonging to the order Erysiphales (Glawe, 2008). Recessively inherited mutant alleles of *Mlo* genes (*mlo*) confer broad-spectrum penetration resistance to powdery mildew pathogens, as in monocotyledonous barley (*Hordeum vulgare*) and the dicotyledonous model plant *Arabidopsis thaliana* (Jørgensen, 1992; Consonni et al., 2006). Genetic analysis has identified several components that are required for *mlo*-mediated resistance, such as the *Ror* (*Required for mlo-specified resistance*) genes in barley, and *PEN* (*PENETRATION*) genes in *Arabidopsis* (Kusch and Panstruga, 2017). However, the exact molecular mechanism underlying *mlo*-mediated resistance remains to be resolved. Non-host resistance is often associated with the failed entry of attacked plant cells by pathogens that are beyond the host range of the particular plant species (Lipka et al., 2008). It was hypothesized that *mlo*-mediated immunity and non-host resistance rely on overlapping molecular pathways since both are associated with unsuccessful host cell entry and some genes (e.g., *Arabidopsis PEN* and barley *Ror* genes) are required for both types of immunity (Humphry et al., 2006). Apart from genetic suppressors of *mlo*-mediated resistance, some chemicals have been identified that partially restore powdery mildew susceptibility in *mlo* genotypes. These include an inhibitor of callose biosynthesis (2-deoxy-D-glucose; (Bayles et al., 1990; Wu et al., 2017)), the actin polymerization inhibitor cytochalasin E (CytE) (Miklis et al., 2007), endosomal trafficking inhibitors (e.g. Brefeldin A and Wortmannin; (Wu et al., 2017)), ribonucleosides, ribonucleoside derivatives, nucleobases, and nucleobase derivatives (Wu et al., 2017) as well as polyamines (e.g. spermidine) (Wu et al., 2017).

The chemical alloxan (5,5-dihydroxyl pyrimidine-2,4,6-trione) belongs to the class of pyrimidones. It is a pyrimidine derivative with substitutions at positions C-2, -4, -5 and -6 by oxo groups, which confers the compound strong oxidative properties. Alloxan became of interest after it was found that the substance can induce diabetes in animals *via* initiating necrosis of pancreatic  $\beta$  cells (Shaw Dunn and Mcletchie, 1943; Peschke et al., 2000). Subsequent studies revealed that the chemical has two distinct functions in this context: On the one hand, it selectively inhibits glucokinase, a glucose sensor of  $\beta$  cells that is responsible for inducing insulin secretion in the pancreas (Meglasson et al., 1986).

On the other hand, it can generate oxygen radicals through redox cycling reactions with its reduction product dialuric acid and reductive substances such as glutathione, resulting in the necrosis of pancreatic  $\beta$  cells (Winterbourn and Munday, 1989). Except for being a diabetogenic agent, alloxan was found to inhibit the activity of O-linked *N*-acetylglucosamine transferase and *N*-acetyl- $\beta$ -D-glucosaminidase, which catalyze the addition and removal of *N*-acetylglucosamine to and from serine or threonine residues of proteins, respectively (Konrad et al., 2002; Lee et al., 2006).

We previously devised a chemical screen to identify chemical suppressors of *mlo* resistance (Wu et al., 2017). In this screen, we identified - among other substances - prototypical nucleoside-derived adenylate cyclase inhibitors (2'-3'-dideoxyadenosine, 2'-5'-dideoxyadenosine and vidarabine) as suppressors of *mlo*-mediated resistance. In an extension of this earlier work, we here report that alloxan, which has been also described as an adenylate cyclase inhibitor in animal (Cohen and Bitensky, 1969) and plant cells (Witters et al., 2005; Ma et al., 2009), is likewise a potent suppressor of *mlo*-based resistance in barley and *Arabidopsis*. We performed a comprehensive set of histochemical and cell biological analyses to explore the molecular basis for the inhibitory effect of alloxan on *mlo* immunity. We discovered that alloxan application results in disassembly of the cytoskeleton, affecting both actin filaments and microtubules. This effect causes a global impairment of cellular transport capacity, as evidenced by a cessation of organelle motility as well as severely affected pathogen attack-associated protein dynamics, callose deposition, and accumulation of reactive oxygen species. These cellular alterations might be the consequence of an early transient oxidative burst generated upon alloxan treatment.

## Results

### **Alloxan and some of its structural analogs are suppressors of *mlo*-mediated powdery mildew resistance in barley**

We selected alloxan (Fig. 1A) as a functional analog of prototypical adenylate cyclase inhibitors (Cohen and Bitensky, 1969) discovered in a previous chemical screen for suppressors of *mlo*-mediated resistance (Wu et al., 2017). Alloxan treatment (5 mM) of barley leaves (*mlo* genotype) significantly increased the penetration success of the barley powdery mildew pathogen *Blumeria graminis* f.sp. *hordei* (*Bgh*) to ~16% compared to ~2% for the water control (Fig. 1B) and enabled the formation of fungal microcolonies (Fig. 1C).

To assess the structural basis for this activity, we tested a series of its chemical analogs, including barbituric acid, isobarbituric acid, uracil, 2(1H)-pyrimidinone, 4,6-dihydropyrimidine, 4(3H)-pyrimidinone and pyrimidine (Table 1), for their ability to break *mlo* resistance. Treatment with barbituric acid (5 mM), uracil (10 mM) and 2(1H)-pyrimidinone (5 and 10 mM) resulted in a statistically significant increase of *Bgh* penetration success to ~13-23%, while the other alloxan analogs were not effective at the concentrations tested (Fig. S1 and Table 1).

To investigate whether alloxan exerts its effect through interfering with known genetic components required for *mlo* resistance, we analyzed its impact on the barley *mlo ror1* double mutant. Besides lacking a functional *Mlo* copy, this double mutant is defective in the gene *Required for mlo-specified Resistance 1* (*Ror1*) and shows a partial relief of *mlo*-mediated resistance compared to the respective *mlo* single mutant (Freialdenhoven et al., 1996). Treatment with alloxan (5 mM) further enhanced the susceptibility of the *mlo ror1* double mutant (entry rate ~51%, Fig. S2). Thus, the effects of alloxan treatment and the *ror1* mutation appear to be additive, suggesting that the chemical probably overcomes barley *mlo* resistance by impairing one or more ROR1-independent pathway(s).

### **Alloxan compromises *mlo*-mediated and non-host resistance in *Arabidopsis***

Next, we tested the effect of alloxan on *mlo*-mediated resistance of *Arabidopsis* against its adapted powdery mildew pathogen, *Golovinomyces orontii*. We first focused on two

independent allelic combinations of the *Arabidopsis mlo2 mlo6* double mutant, which exhibits partial penetration resistance to *G. orontii* with a host cell entry rate of ~20% (Consonni et al., 2006). Similar to barley *mlo* genotypes, alloxan treatment significantly increased the penetration success of *G. orontii* to ~21-23% in comparison to ~5% for the water control for both mutants (Fig. S3A and S3B; note that experimental stress causes a general reduction in entry rates in pharmacological inhibitor experiments). We then assessed the effect of alloxan on two independent *Arabidopsis mlo2 mlo6 mlo12* triple mutants. Both triple mutants are fully resistant to *G. orontii* with host cell entry rates of ~0-1% (Consonni et al., 2006; Acevedo-Garcia et al., 2017). Treatment with alloxan led to an increase of penetration success to ~14% (*mlo2-5 mlo6-2 mlo12-1*; Fig. 2A and C) and ~32% (*mlo2-6 mlo6-4 mlo12-8*; Fig. S3C and S3D), compared to 0% for the water control for both triple mutants.

Given the commonalities between non-host resistance and *mlo*-mediated resistance against powdery mildew fungi (Humphry et al., 2006), we further tested the effect of alloxan in an incompatible interaction between *Arabidopsis* and *Bgh*, which is a non-adapted powdery mildew pathogen for this plant species. Treatment with alloxan increased the penetration success of *Bgh* to ~37% compared to ~0% for the water control (Fig. 2B). In addition, application of the chemical also facilitated the formation of *Bgh* microcolonies (Fig. 2D).

### **Alloxan reduces callose deposition and interferes with hydrogen peroxide accumulation in powdery mildew-attacked epidermal cells**

Deposition of callose, a  $\beta$ -1,3 glucose polymer, beneath attempted fungal penetration sites is thought to generate physical barriers by local plant cell wall reinforcement (Voigt, 2014). To investigate whether localized pathogen-induced callose deposition is affected by alloxan treatment, we evaluated this parameter in epidermal cells of the four types of plant-powdery mildew interactions analyzed before (Fig. 1 and 2, Fig. S3). The compound significantly reduced callose deposition at attempted fungal entry sites in all four types of interactions (from ~20-60% for the solvent control to less than 5% in the alloxan-treated samples; Fig. 3 and Fig. S4).

During non-host resistance of *Arabidopsis* against *Bgh*, a small portion (~5%) of epidermal cells that are successfully penetrated by the fungus typically initiate post-invasion resistance characterized by a hypersensitive cell death response (Lipka et al., 2005). Usually, a burst of reactive oxygen species (ROS) precedes the commencement of cell death (Torres et al., 2006). To study the impact of alloxan on ROS production during the non-host interaction of *Arabidopsis* and *Bgh*, we scored the accumulation of hydrogen peroxide (H<sub>2</sub>O<sub>2</sub>) in epidermal cells challenged with *Bgh* at 48 hours post inoculation (hpi). Six types of H<sub>2</sub>O<sub>2</sub> accumulation patterns were discerned microscopically (designated type I-VI; Fig. S5A and B). In comparison to the water treatment in which type I (57%), type II (23%) and type III (18%) dominate, H<sub>2</sub>O<sub>2</sub> accumulation was diminished in a statistically significant manner by alloxan application, and type III (56%) and type VI (42%) were the prevalent forms of H<sub>2</sub>O<sub>2</sub> accumulation (Fig. S5C).

### **Alloxan interferes with the mobility and morphology of cellular organelles and the recruitment of the PEN1/SYP121 t-SNARE protein to attempted fungal entry sites**

Some cellular organelles as well as a subset of proteins (e.g., the t-SNARE PEN1/SYP121) were reported to accumulate beneath attempted fungal penetration sites, presumably to facilitate antifungal defense responses (Bhat et al., 2005; Yang et al., 2014). To explore the possibility that alloxan exerts its function through interfering with the dynamics of organelles and defense proteins, we tested the compound on a series of *Arabidopsis* transgenic marker lines expressing green fluorescent protein (GFP)-tagged proteins localizing to various organelles and a line expressing GFP-tagged PEN1. Treatment with alloxan severely impeded the motility of peroxisomes, leading to near-complete cessation (Fig. 4A, Movie S1), and affected the dynamics of endosomes (Fig. 4B, Movie S2) and the endoplasmic reticulum (Fig. 4C, Movie S3). While peroxisome morphology remained essentially unaltered by alloxan exposure, the compound influenced endosome morphology, resulting in smaller, less regularly shaped and more granular entities (Fig. 4B, Movie S2). Similarly, the endoplasmic reticulum exhibited altered morphology upon alloxan application, with many more small-sized hexagonal honeycomb-like sections present (Fig. 4C, Movie S3). Furthermore, the chemical

prevented recruitment of these organelles and GFP-PEN1, which forms a ternary SNARE complex with its partner proteins and is important for antimicrobial secretory processes to sites of attempted pathogen entry (Kwon et al., 2008). Instead, GFP-PEN1 congregated into small unevenly shaped protein bodies scattered randomly throughout the cytosol and showed no motility when imaged at 18 hpi or 48 hpi (Fig. 4D, Fig. S6A and B, Movie S4). To investigate whether these GFP-PEN1 protein assemblies are still part of a dynamic protein pool, we performed a fluorescence recovery after photobleaching (FRAP) experiment. Following bleaching, GFP-PEN1 protein bodies showed no recovery within a period of 2 h (Fig. S6C and D), suggesting these protein aggregates are likely stationary and non-functional.

### **Alloxan disrupts cytoskeleton integrity and architecture in plants, but not in fungal or human cells**

Given that the motility of cellular organelles largely relies on the cytoskeleton (and its associated motor proteins), we hypothesized that this intracellular network could be a potential direct or indirect target of alloxan. To explore this possibility we first tested the compound on an *Arabidopsis* transgenic line constitutively expressing a GFP-tagged actin-binding protein (GFP-fABD2) (Voigt et al., 2005b). Confocal microscopy revealed that thick actin filament cables are present at 18 hpi in epidermal cells treated with water (Fig. 5A). By contrast, reticular networks of thin actin filaments with node-shaped protein bodies dispersed in-between formed at 18 hpi in epidermal cells treated with alloxan (Fig. 5A). We observed a similar differential pattern of actin organization at 40 hpi (Fig. S7), indicating that the chemical causes prolonged perturbation of the actin filament network. In order to investigate whether the substance affects also the dynamics of actin filaments upon fungal challenge, we examined their behavior over a period of 30 min starting from 18 hpi. Thick actin cables exhibited focal accumulation, yet showed active dynamics at incipient penetration sites in epidermal cells of leaves treated with water (Fig. 5B). By contrast, actin cables remained disrupted, unfocussed and exhibited no dynamics during the 30 min period in epidermal cells of alloxan-treated leaves (Fig. 5B).

We selected the renowned inhibitor CytE, which is known to interfere with the organization and function of actin filaments (Cooper, 1987), for comparison with alloxan. In contrast to the peculiar pattern induced by alloxan application (thin filaments and node-shaped protein aggregates), bundles of actin filaments were completely fragmented at 18 hpi in epidermal cells of leaves treated with 10  $\mu$ M CytE (Fig. 5A). However, unlike alloxan (Fig. 2, Fig. S3), treatment with CytE did not compromise powdery mildew resistance in the *Arabidopsis mlo2 mlo6* double and *mlo2 mlo6 mlo12* triple mutants (Fig. S8).

We next explored whether alloxan analogs, which in part also partially break *mlo* resistance in barley (Fig. 1 and Table 1), also impair actin cytoskeleton architecture in *Arabidopsis* cotyledons. We found that similar to alloxan, barbituric acid results in disruption of actin filament arrays at concentrations  $\geq 10$  mM, whereas all other substances tested showed either little or no effect (Fig. S9). We then examined in the same assay a subset of the chemicals that were previously found to affect *mlo* resistance in barley (Wu et al., 2017). None of these compounds (2',3'-dideoxyadenosine, 2-deoxy-D-glucose, spermine, uridine and guanosine) affected actin integrity or architecture at the concentrations tested (up to 25 mM; Fig. S10).

To characterize alloxan activity further, we next quantified the architecture and organization of actin filament arrays in cells of hypocotyls in the GFP-fABD2 *Arabidopsis* actin marker line, with an established assay for the quantitative assessment of filament bundling (skewness) and abundance (percentage of occupancy or density) (Henty-Ridilla et al., 2013). Similar to the effect caused by the positive control CytD, short-term treatment with alloxan for 15 min significantly reduced the density of filament arrays and increased the extent of bundling of actin filaments in a dose-dependent manner (Fig. 5C-E). This outcome was also seen at 1 h and 2 h after application of the compound (Fig. S11).

To investigate the putative molecular basis for the actin filament-destabilizing activity of alloxan, we tested its influence in an *in vitro* actin filament depolymerization experiment using a co-sedimentation assay with rabbit actin. Treatment with different concentrations (1  $\mu$ M–1 mM) did not increase the rate of depolymerization of actin filaments compared to that of the solvent control after incubation for 2 h (Fig. S12). In order to examine the activity of alloxan in the assembly of globular (G-) actin into filaments (F-actin), we

monitored its influence on the process of actin polymerization using a fluorometry-based assay. Treatment with different concentrations (1  $\mu\text{M}$ –100  $\mu\text{M}$ ) did not interfere with the assembly of G-actin compared to the control over a period of 900 s (Fig. S13).

With the aim of investigating the effect of alloxan on the other structural component of the plant cytoskeleton, the microtubules, we applied the compound to cotyledons of an *Arabidopsis* transgenic line expressing a GFP-tagged version of  $\alpha$ -tubulin (GFP-TUA6). In comparison to the respective water control, alloxan treatment led to a disintegration of the microtubular network into protein aggregates in epidermal cells at 6 h after incubation (Fig. S14).

Given the pronounced effect of alloxan on plant cytoskeleton integrity and architecture, we also tested the compound on fungal and human cells to address the question whether the substance might have a conserved cellular target. For the former we took advantage of two fungal species, the basidiomycete maize pathogen *Ustilago maydis* and the ascomycete wheat pathogen *Zymoseptoria tritici*, for which transgenic actin marker lines were available and that unlike powdery mildews can be tested by *in vitro* growth assays. In the case of these two fungi, alloxan application had little effect on the actin cytoskeleton, did not cause any discernible growth reduction of the fungi, and also did not impact their survival rate at any of the concentrations tested (Fig. S15). Likewise, the substance had only mild effects on the actin cytoskeleton arrangement in cells of a human vulvar carcinoma cell line and did not affect microtubules or the keratin network in these cells (Fig. S16). The marked effect of alloxan on cytoskeleton integrity and architecture thus appears to be a plant-specific phenomenon.

### **Alloxan induces hydrogen peroxide production and increases plasma membrane permeability in *Arabidopsis***

Previously, alloxan was found to promote diabetes in animals, partially through its toxicity on pancreatic  $\beta$  cells *via* accumulation of ROS (Oberley, 1988; Winterbourn and Munday, 1989). The chemical was also applied as a ROS inducer to study the role of ROS during plant tissue development and differentiation (Liptáková et al., 2012; Benitez-Alfonso et al., 2009). We therefore assessed  $\text{H}_2\text{O}_2$  accumulation in cotyledons and leaves of *Arabidopsis* after infiltration with alloxan *via* histochemical staining with 3,3'-

diaminobenzidine (DAB). Incubation of cotyledons with the substance for 3 h significantly increased H<sub>2</sub>O<sub>2</sub> levels (~37% of the leaf area) compared to the water control (~11% of the leaf area; Fig. 6A and 6B). We further performed DAB staining in the GFP-FABD2 actin marker line at 5 h after infiltration of cotyledons with alloxan. We observed intense punctate DAB staining in the epidermal cells of these cotyledons, coincident with a disassembly of actin filaments in the same cells (Fig. 6C). We next measured H<sub>2</sub>O<sub>2</sub> levels in rosette leaves of *Arabidopsis* infiltrated with alloxan at multiple time points. Treatment with the chemical significantly increased H<sub>2</sub>O<sub>2</sub> accumulation in mature leaves at 6 h after infiltration (~21% of the leaf area) compared to the water control (~13% of the leaf area, Fig. 6D and E). This increase was transient since at later time points (12 and 24 h) alloxan-treated leaves did not differ from control leaves (Fig. 6D and E).

Given that cellular membranes are highly sensitive to ROS, we further explored the impact of alloxan on plasma membrane integrity of epidermal cells of *Arabidopsis* cotyledons and rosette leaves using propidium iodide staining. Alloxan enhanced plasma membrane permeability in both cotyledons and rosette leaves, as indicated by an increase in red fluorescence inside epidermal cells (Fig. S17).

### **Glucose pretreatment protects actin filaments from disintegration by alloxan**

Studies in animals revealed that alloxan is transported into pancreatic  $\beta$  cells through a glucose transporter, possibly due to its structural similarity to glucose (Weaver et al., 1978; Elsner et al., 2002). To analyze whether the passage of the chemical from the apoplast into plant cells may also depend on glucose transporters, we established a competition experiment in which we pre-incubated the cotyledons of *Arabidopsis* with various concentrations of D-glucose for 2 h prior to the addition of alloxan. Pre-incubation with D-glucose (250 mM) protected the actin filaments from the disassembly by alloxan at 6 h after infiltration, while incubation with D-glucose (250 mM) alone did not affect actin filament architecture (Fig. S18).

## Discussion

In this study, we identified alloxan and some of its structural analogs as chemical suppressors of *mlo*-mediated powdery mildew resistance in barley and *Arabidopsis* and non-host resistance of *Arabidopsis* against *Bgh*. In plant cells, the chemical causes pleiotropic effects such as a transient ROS burst (Fig. 6D and E), enhanced plasma membrane permeability (Fig. S17), disassembly of the cytoskeleton (Fig. 5) associated with a cessation of organelle motility (Fig. 4, Movies S1-S3), changes in organelle morphology (Fig. 4, Movies S1-S3) and altered protein dynamics (Fig. 4, Fig. S6 and Movie S4). The affected cells must nevertheless be still alive and at least partially responsive since they support invasive growth of an obligate biotrophic phytopathogen that relies on living host cells and intact host physiology.

The fact that four chemically-related substances (alloxan, barbituric acid, uracil and 2(1H)-pyrimidinone; Table 1) affect *mlo* resistance suggests that these four compounds may share (a) common molecular target(s) that are critical for this type of immunity. The comparatively high concentrations (mM range) of the inhibitory substances needed are not unusual for intact plant systems, and putative reasons for this have been discussed before (Wu et al., 2017; Planchais et al., 2000). The plant cell wall is a physical barrier for the uptake of any chemical agent, especially in tissue context. The quantity of an inhibitor required to block an activity in whole plant organs is often 10-fold higher than that required for plant cells in suspension culture. Required concentrations can also differ by one order of magnitude for a given inhibitor between different plant species (Planchais et al., 2000). Furthermore, the stability of chemicals in the apoplastic space and/or cytoplasm as well their membrane permeability are key parameters that may affect their inhibitory activity and thus dictate the required concentrations (Wu et al., 2017).

In barley, we noted a comparatively narrow window of effective concentration for alloxan, with a weak (if any) effect at 1 mM, a strong effect at 5 mM and even a negative impact on fungal host cell penetration at 10 mM (Fig. 1B, Fig. S2). This was true for both the *mlo-5* and *mlo-5 ror1-5* genotypes, and the strong decline at 10 mM was particularly evident for the *mlo-5 ror1-5* double mutant (Fig. S2). A similar drop in host cell entry rates upon exposure to 10 mM alloxan was not seen in the case of *Arabidopsis* in our experiments

(Fig. 2A and 2B; Fig. S3). We thus conclude that elevated alloxan concentrations may affect viability of barley host cells, which is required to sustain pathogenicity of the obligate biotrophic *Bgh* pathogen. Alternatively, excessive alloxan concentrations might also impede the fungus itself. Notably, in the context of the *Arabidopsis-Bgh* constellation, 10 mM alloxan was the most effective concentration, and a strong decline of host cell entry was only seen at 25 mM (Fig. 2B), which may argue against the latter explanation. However, it has to be considered that the uptake, distribution and stability of alloxan could differ between the barley and *Arabidopsis* plant systems, which may account for the observed differences.

Apart from affecting the resistance of the barley *mlo* mutant, alloxan is also to compromise partially resistance in the *Arabidopsis mlo2 mlo6 mlo12* triple mutant (Fig. 2A and 2C). This effect is remarkable as so far all genetic and pharmacological attempts to overcome this highly effective type of immunity failed (Consonni et al., 2006; Wu et al., 2017; Kuhn et al., 2017). By contrast, several chemical inhibitors have been reported to break partially *mlo* resistance in barley (Wu et al., 2017; Bayles et al., 1990; Miklis et al., 2007). It can thus be hypothesized that alloxan either targets a cellular component that is key for resistance of the *mlo2 mlo6 mlo12* triple mutant or that the compound affects multiple defense pathways in parallel, including actin cytoskeleton function, which is known to be critical for *mlo* resistance in barley (Miklis et al., 2007). However, given that CytE, a renowned and potent actin polymerization inhibitor, failed to impair resistance of the *Arabidopsis mlo2 mlo6 mlo12* triple mutant (Fig. S8), the resistance-breaking activity of alloxan cannot solely rely on its interference with the actin cytoskeleton.

Since alloxan does not affect actin polymerization/depolymerization *in vitro* (Fig. S12 and S13), its activity is likely an indirect effect that might be caused by interaction of the chemical with other cellular components *in vivo*. This notion is further supported by the fact that alloxan treatment results in disintegration of both actin filaments (Fig. 5) and microtubules (Fig. S14), which renders direct interactions with cytoskeletal components unlikely. Given its broad cytoskeleton-affecting activity, it is plausible to assume that alloxan suppresses multiple types of plant defense since these intracellular networks are critical for many cellular processes. The fact that the substance also impedes the pathogen-triggered subcellular redistribution of the PEN1/SYP121 t-SNARE (Fig. 4D, Fig.

S6), which was previously shown to occur independently of the actin cytoskeleton (Underwood and Somerville, 2013), further supports the idea that alloxan affects additional processes different from cytoskeleton organization.

While the present study focused on *mlo* resistance in barley and *Arabidopsis* and nonhost resistance to *Bgh* in *Arabidopsis*, it will be interesting to explore the impact of alloxan on other types of resistance and pathogens in the future. These could comprise resistance (*R*) gene-conditioned powdery mildew immunity in barley (e.g. *Mla* resistance; (Jørgensen, 1994)) or *RPW8*-mediated powdery mildew immunity in *Arabidopsis* (Xiao et al., 2001). In a previous study, the polyamine spermine was found to affect both, barley *mlo*-mediated and *Mla1*-conditioned resistance against *Bgh*. Notably, spermine was not only effective in the context of these barley-*Bgh* interactions, but also increased barley susceptibility to the hemibiotrophic rice blast pathogen, *Magnaporthe oryzae* (Wu et al., 2017). It will thus be informative to study whether alloxan likewise affects interactions with other (hemi-)biotrophic pathogen species such as e.g. the interaction of *Arabidopsis* with the bacterial pathogen *Pseudomonas syringae* or the oomycete *Hyaloperonospora arabidopsidis*.

We found that alloxan induces an early (at 6 h after application) transient H<sub>2</sub>O<sub>2</sub> burst in both cotyledons and leaves of *Arabidopsis* (Fig. 6), but reduces H<sub>2</sub>O<sub>2</sub> accumulation at fungal entry sites when scored at 48 hpi (Fig. S5), which upon first view seem to be contradictory outcomes. However, the functional connection between ROS production and the plant defense machinery is complex and multifaceted. ROS have been assigned a dual role in the context of plant-microbe interactions, serving on the hand as signaling molecules and on the other hand as toxic molecules with strong oxidant power (Camejo et al., 2016). ROS accumulate transiently upon exposure of plant cells to microbe-associated molecular patterns (MAMPs) (Bigeard et al., 2015) and in the context of pathogen-triggered cell death, e.g. during the hypersensitive response (HR) following attack by avirulent pathogens (Zurbriggen et al., 2010). The main enzymes involved in the production of ROS in the context of plant defense are apoplastic peroxidases and plasma membrane-localized NADPH oxidases, whereas intracellular ROS are mainly produced in chloroplasts and peroxisomes/glyoxysomes and to a lesser degree in mitochondria (Qi et al., 2017). At present, we do not know whether the transient ROS

burst seen at 3-6 h following alloxan application involves the ROS-generating cellular machinery or is an effect of the chemical itself, as known from mammalian pancreatic  $\beta$  cells. In the latter cell type, alloxan generates reactive oxygen species (ROS) in the presence of intracellular thiols, especially glutathione, in a cyclic redox reaction with its reduction product, dialuric acid. Autoxidation of dialuric acid generates superoxide radicals, hydrogen peroxide and, in a final iron-catalysed reaction step, hydroxyl radicals (Lenzen, 2008).

The short transient ROS burst triggered by MAMPs has been shown to cause remodeling of the actin cytoskeleton, resulting in an increase of overall filament abundance (Li et al., 2017) – an outcome that is quite different from alloxan-induced cytoskeleton disassembly (Fig. 5). We detected that the disruption of actin filaments temporally and spatially coincides with the formation of  $H_2O_2$  in the cells of cotyledons after alloxan infiltration (Fig. 6C). We thus speculate that the temporary alloxan-induced  $H_2O_2$  burst could be causative for subsequent disintegration of the cytoskeleton, given that high ROS levels can result in the crosslinking of proteins into aggregates, which may lead to their malfunction (Davies, 1987; Davies and Delsignore, 1987; Davies et al., 1987). The reason for the opposite effects of a MAMP- and an alloxan-triggered ROS burst regarding actin filament architecture could be related to the type, intensity, duration and/or subcellular localization of ROS production.

We hypothesize the following scenario for the cellular activity of alloxan: An early (at 6 h) temporary  $H_2O_2$  burst after infiltration may result in an impairment of cytoskeleton integrity and architecture, possibly combined with other cellular perturbations. This could result in the failure of several cellular processes that are critical for plant defense, e.g. the motility of cellular organelles, eventually resulting in a (partial) breakdown of resistance at a later time point (at 24-48 hpi). This could also explain the reduced ROS burst at fungal entry sites, given that the cytoskeleton is critical for signal transduction and vesicle trafficking, which are both necessary for effective ROS production.

## Materials and Methods

### Plant materials and growth conditions

Barley (*H. vulgare*) lines *mlo-3* (in the background of cv. Ingrid; (Büschges et al., 1997) and *mlo-5 ror1-5* (in the background of cv. Ingrid; (Freialdenhoven et al., 1996)) were used for this study. The *A. thaliana* lines used in this work include accession Col-0 (wild-type), *mlo2-5 mlo6-2* and *mlo2-6 mlo6-4* double mutants (in Col-0 background; (Consonni et al., 2006) and unpublished data), and the *mlo2-5 mlo6-2 mlo12-1* and *mlo2-6 mlo6-4 mlo12-8* triple mutants (in Col-0 background; (Consonni et al., 2006; Acevedo-Garcia et al., 2017)). Transgenic *Arabidopsis* reporter lines (in Col-0 background unless otherwise stated) include the peroxisome marker line p35S::GFP-PTS1 (kindly provided by Nikolaus Schlaich), the endosome marker line p35S::GFP-2xFYVE (Voigt et al., 2005a), the ER GFP marker line p35S::SP-GFP-HDEL (kindly provided by Nikolaus Schlaich), the actin marker line p35S::GFP-fABD2 (Voigt et al., 2005b), the tubulin reporter line p35S::GFP-TUA6 (kindly provided by Nikolaus Schlaich) and the PEN1-GFP line p35S::GFP-PEN1 (in *pen1-1* background; (Collins et al., 2003)). All barley plants were grown at 23 °C and 16 h light/8 h darkness in a controlled environment. All *Arabidopsis* plants were grown at 22 °C and 8 h light/16 h darkness in a controlled environment.

### Fungal materials and growth conditions

*Bgh* (isolate K1) was propagated on barley cv. Margret, and *G. orontii* was propagated on susceptible *Arabidopsis* Col-0 and mutant *eds1-2* (in Col-0 background; (Bartsch et al., 2006)). Powdery mildew inoculations of plant samples were performed at medium to high spore densities of ca. 20-50 conidia mm<sup>-2</sup>. *U. maydis* strains FB1, FB2Fim2G and AB33GLAct (Theisen et al., 2008; Schuster et al., 2012; Banuett and Herskowitz, 1989), grown overnight at 28 °C in complete medium (Holiday, 1974) containing 1% (w/v) glucose by shaking at 200 revolutions per minute (rpm). *Z. tritici* strains IPO323, IPO323\_Fim1-eGFP and IPO323\_Lifact-ZtGFP (Kilaru et al., 2015; Kilaru et al., 2017; Kema and van Silfhout, 1997) were grown for two days in YG media (yeast extract, 10 g L<sup>-1</sup>; glucose, 30 g L<sup>-1</sup>) at 18 °C by shaking at 200 rpm.

### Human vulvar carcinoma cell line and growth conditions

The single cell clone AK13-1 stably expressing keratin 13-eGFP from the vulvar

carcinoma A431 cell line was described previously (Windoffer and Leube, 1999). The cells were cultivated at 37 °C and 5% CO<sub>2</sub> humidified atmosphere in Dulbecco's Modified Eagle Medium (DMEM) containing L-alanyl-glutamine (Sigma-Aldrich, Munich, Germany) and 10% (v/v) fetal bovine serum (FCS) SeraPlus (PAN Biotech, Aidenbach, Germany). For passaging, cells were washed with phosphate-buffered saline (PBS) without Ca<sup>2+</sup>/Mg<sup>2+</sup> (Sigma-Aldrich) and thereafter trypsinized in a solution of PBS without Ca<sup>2+</sup>/Mg<sup>2+</sup> (Biochrom, Berlin, Germany) containing 0.25% (w/v) trypsin (Biochrom) supplemented with 0.02% (w/v) ethylenediaminetetraacetic acid (Sigma-Aldrich). Cells were passaged two times per week after reaching confluence for at least one day.

### Chemicals

Chemicals were purchased from the following companies: Alloxan (alloxan monohydrate, A7413, Sigma-Aldrich), barbituric acid (2,4,6-trihoxypyrimidine, 185698, Sigma-Aldrich), isobarbituric acid (2,4,5-trihoxypyrimidine, AB133691, abcr GmbH Karlsruhe, Germany), 4,6-dihoxypyrimidines (AB115988, abcr GmbH), uracil (2,4[1H,3H]-pyrimidinedione, U1128, Sigma-Aldrich), 2(1H)-pyrimidinone (2[1H]-pyrimidinone hydrochloride, H57408, Sigma-Aldrich), 4(3H)-pyrimidinone (AB125837, abcr GmbH), pyrimidine (sc-272129, Santa Cruz Biotechnology, Heidelberg, Germany), cytochalasin E (C2149, Sigma-Aldrich), cytochalasin D (C8273, Sigma-Aldrich), latrunculin B (AG-CN2-0031-M001, AdipoGen Life Sciences, Liestal, Switzerland). Note that cytochalasin D (CytD) and cytochalasin E (CytE) are structurally similar mycotoxins that inhibit actin filament polymerization in a comparable manner (by capping filament ends) and can thus be used interchangeably in most bioassays. We used both types in our study to allow comparison with previous data generated with the respective cytochalasins. Alloxan and all other chemicals were dissolved as stock solutions in deionized water, methanol or cell culture medium and diluted to the final concentrations as indicated. For most experiments, alloxan was used in aqueous solution, prepared as 100 mM stock in deionized water and diluted in water for application to plant specimens. Exceptions were as follows: For the experiments with *U. maydis* and *Z. tritici*, alloxan stock solution (200 mg mL<sup>-1</sup>) was prepared in methanol and the compound used at 1 mg/ml in the medium (0.5% methanol). For the experiments with the human vulvar carcinoma A431 cell line, alloxan solutions were freshly prepared in cell culture medium.

## Application of chemicals to plant specimens

Application of chemicals was performed *via* a vacuum-infiltration procedure. In case of barley, the lower (abaxial) epidermis of excised first leaves (seven to eight days old) was carefully peeled off using forceps. Leaves were then floated on solutions of the respective compounds in Petri dishes, with the abaxial side in contact with the solutions. Thereafter, samples were vacuum-infiltrated for ~20 min in a desiccator. Subsequently, the upper (adaxial) epidermis of the leaves was inoculated with conidiospores from *Bgh* by flapping the inoculum above an inoculation box, ensuring an equal inoculation density. In the case of *Arabidopsis*, detached rosette leaves (four to five weeks old) were placed into a 2 ml reaction tube containing solutions of the respective compounds. Petioles were immersed in the solutions and samples then vacuum-infiltrated for 40 min. Leaves were kept *in situ* for 1 h for resting before they were transferred onto 1% agar plates (containing 85  $\mu$ M benzimidazole; Sigma-Aldrich) and inoculated with conidiospores from *G. orontii* or *Bgh* by brushing inoculum on the top of the adaxial side of the leaves. For both barley and *Arabidopsis*, leaves were fixed in a destaining solution (a 1:3 mixture of acetic acid and ethanol) at 48 hpi, and epiphytic fungal structures stained with Coomassie Brilliant Blue R-250 (Carl Roth C.I. 42660, Karlsruhe, Germany; 0.05% in 45% (v/v) methanol/10% (v/v) acetic acid) for microscopic analysis. Host cell entry was scored by light microscopy as the proportion of germinated conidia that succeeded in the formation of secondary hyphae. Micrographs of fungal infection structures were captured with a Keyence BZ-9000 digital microscope (Keyence, Osaka, Japan).

For chemical treatment of *Arabidopsis* cotyledons, seedlings (six to seven days old) cultured in liquid 1x Murashige & Skoog (MS) medium were immersed in the medium with the addition of respective chemicals to appropriate final concentrations. Subsequently, samples were vacuum-infiltrated for 10 min.

## Callose staining

Histochemical staining of callose was performed with aniline blue. Infected leaf material was first destained with a destaining solution (1:3 mixture of acetic acid and ethanol) for 2-3 d. Then, leaves were rinsed with water, transferred using to aniline blue (0.01% (w/v) in water; 415049, Sigma-Aldrich) staining solution, and kept in the dark ON at room temperature. Subsequently, samples were mounted on a glass slide and analyzed with a

Keyence BZ-9000 digital microscope equipped with a DAPI (4',6-diamidin-2-phenylindole) emission filter under ultraviolet (UV) light excitation.

### **Hydrogen peroxide staining**

Histochemical *in situ* detection of H<sub>2</sub>O<sub>2</sub> in mature *Arabidopsis* rosette leaves by staining with 3,3'-diaminobenzidine (DAB) was performed as described previously (Thordal-Christensen et al., 1997). Briefly, 1 mg mL<sup>-1</sup> 3,3'-diaminobenzidine tetrahydrochloride hydrate (D5637, Sigma-Aldrich) solution was made by dissolving the powder in deionized water and adjusting the pH by adding Na<sub>2</sub>HPO<sub>4</sub> to a final concentration of 10 mM. Detached leaves were immersed in the solution in a 15 ml plastic tube and three times vacuum-infiltrated in a desiccator for 15 min. Thereafter, samples were kept overnight in darkness. For staining of cotyledons, *Arabidopsis* seedlings were immersed in the DAB solution in a 2 ml reaction tube and vacuum-infiltrated in a desiccator for 10 min. Subsequently, samples were kept in darkness for 6-8 h before microscopy.

The quantification of H<sub>2</sub>O<sub>2</sub> levels in leaves and cotyledons of *Arabidopsis* was performed as follows: destained leaves were mounted on glass slides and images were captured with a stereomicroscope system (M205 FA; Leica, Wetzlar, Germany); destained cotyledons were mounted on glass slides and images were taken using a Keyence BZ-9000 digital microscope. The respective images were first transformed into black and white color mode and then the relative areas of black color (DAB-positive staining) were calculated using Image J (<https://imagej.nih.gov/ij/>) software.

### **Confocal laser scanning microscopy (CLSM)**

CLSM was performed with a Leica SP8 microscope equipped with the LAS-X software package, as recommended by the manufacturer. Leaves of *Arabidopsis* were fixed onto glass slides by sticky double-sided tape, and cotyledons were mounted on glass slides with deionized water and sealed with a glass cover slide. Microscopy was performed using the 20x dry or 63x water immersion objective. The following excitation and emission wavelengths were used: propidium iodide, excitation 535 nm, emission 610-670 nm; GFP, excitation 488 nm, emission 505-555 nm. The images displaying both green fluorescence of *Arabidopsis* epidermal cells and red fluorescence of stained fungal structures were generated with the sequential scanning function. For the Fluorescence Recovery After

Photobleaching (FRAP) assay, a region of interest (ROI) around the aggregates of GFP-PEN1 was bleached 25–50 times using the 488 nm argon laser at 100% intensity. Bleaching time for each round varied from 2.5 to 5 seconds, depending on the size of the ROI. Before and after bleaching, images were collected with 5% laser intensity in order to minimize the effect of photobleaching during the imaging process. Images were captured every five minutes after the bleaching with the same settings.

### **Actin architecture assay**

Epidermal cells from 3-d-old dark-grown hypocotyls of the transgenic *Arabidopsis* p35S::GFP-fABD2 actin marker line were imaged by variable-angle epifluorescence microscopy (VAEM) using a total internal reflection fluorescence (TIRF) illuminator on an IX-71 microscope equipped with a 60x/1.45 PlanApo TIRF objective (Olympus, Center Valley, USA). Images were captured with an electron-multiplying CCD camera (ORCA-EM C9100-12; Hamamatsu Photonics, Bridgewater, USA). For actin architecture quantitative analysis, the density, or percentage of occupancy, of actin filament arrays and the extent of bundling (skewness) were analyzed as described previously (Henty-Ridilla et al., 2014).

### **Actin co-sedimentation assay**

A high-speed co-sedimentation assay was employed as described previously (Xiang et al., 2007) with slight modifications. Rabbit skeletal muscle actin (AKL99, Cytoskeleton, Denver, USA) was suspended in Buffer G (5 mM Tris pH 8.0, 0.2 mM ATP, 0.2 mM CaCl<sub>2</sub>, 0.5 mM DTT) and cleared by ultracentrifugation at 100,000 x g for 10 min at 4°C. Preformed F-actin (4 μM) was made by adding 1/9 volume of 10x polymerization buffer (500 mM KCl, 50 mM MgCl<sub>2</sub> and 5 mM ATP) to the 4 μM G-actin sample and incubation at 4°C for 16 h. Preformed F-actin (4 μM) was incubated with various concentrations of alloxan at room temperature for 2 h. The samples were then centrifuged at 100,000 g for 1 h, and the resulting pellets and supernatants were analyzed by SDS-PAGE. Images of the SDS-PAGE were taken by a Gel Doc<sup>TM</sup> XR<sup>+</sup> imaging system (Bio-Rad, Munich, Germany), and the percentage of actin was calculated by quantification of band intensities using the Bio-Rad protein analyzing software.

### **Actin polymerization assay**

A pyrene-actin polymerization assay was performed as described previously (Huang et al., 2003) with slight modifications. Rabbit skeletal muscle actin (AKL99, Cytoskeleton) and pyrene labeled-rabbit skeletal muscle actin (AP05, Cytoskeleton) was suspended in buffer G (5 mM Tris pH 8.0, 0.2 mM ATP, 0.2 mM CaCl<sub>2</sub>, 0.5 mM DTT, and 0.1 mM NaN<sub>3</sub>) and cleared by ultracentrifugation at 140,000 x g for 30 min at 4 °C. Pyrene-actin (10%) was added to unlabeled actin and the mixture was converted to Mg<sup>2+</sup>-actin by addition of 0.2 mM EGTA and 50 µM MgCl<sub>2</sub>. Actin polymerization was initiated by mixing Mg<sup>2+</sup>-actin (at a final concentration of 3 µM) with 10x polymerization buffer (500 mM KCl, 10 mM MgCl<sub>2</sub>, 10 mM EGTA, and 100 mM imidazole-HCl, pH 7.0) in the presence of various concentrations of alloxan or cytochalasin D (C8273, Sigma-Aldrich) suspended in buffer G. Actin assembly was monitored by measuring fluorescence intensity of pyrene using a PTI Quantamaster spectrofluorometer (QM-2000-SE, Photon Technology International, South Brunswick, USA) at 1 s intervals with excitation and emission wavelengths of 365 nm and 407 nm, respectively.

### **Microscopic analyses in *Ustilago maydis* and *Zymoseptoria tritici***

For microscopy, ON grown cells were incubated with 1 mg mL<sup>-1</sup> alloxan (stock 200 mg mL<sup>-1</sup> in methanol) or an equivalent volume of methanol for 24 h at 28 °C (*U. maydis*) and 18 °C (*Z. tritici*). Fluorescence microscopy was performed as previously described (Schuster et al., 2011). In brief, treated cells were placed onto a 2% (w/v) agar cushion for direct observation using a motorized inverted microscope (IX81; Olympus, Hamburg, Germany), equipped with a PlanApo 100x/1.45 Oil TIRF objective (Olympus, Hamburg, Germany). The green fluorescent tag was excited using a VS-LMS4 Laser Merge System with solid-state laser (488 nm 75 mW; Visitron Systems, Puchheim, Germany). To visualize actin cables, Z stacks were generated by using an objective piezo (Piezosystem Jena GmbH, Jena, Germany). Actin patch dynamics were analyzed in kymographs, derived from image sequences of 100 to 250 frames at 150 ms exposure time. Images were captured using a CoolSNAP HQ2 camera (Photometrics/Roper Scientific, Tucson, USA). All parts of the system were under the control of the software package MetaMorph (Molecular Devices, Wokingham, UK). Image processing and quantitative analysis was performed with MetaMorph.

## **Fungal growth/toxicity assay**

To assess the toxicity of alloxan onto *U. maydis* and *Z. tritici*, ON cultures were grown as described above. For *U. maydis* agar plates with complete medium supplemented with 1% glucose and different concentrations of alloxan were prepared and 5  $\mu$ l of different dilutions of the ON cell culture ( $OD_{600}$  1.0; 0.1; 0.01; 0.001; 0.0001) were dropped and incubated for 18 h at 28 °C. *Z. tritici* IPO323 (Kema and van Silfhout, 1997) was grown on YPD plates (yeast extract, 10 g L<sup>-1</sup>; peptone, 20 g L<sup>-1</sup>; glucose, 20 g L<sup>-1</sup>; agar, 20 g L<sup>-1</sup>) for 5 d at 18 °C. Cells were harvested and a cell/water suspension was generated and adjusted to an  $OD_{600}$  of 1.0. YPD agar plates with different concentrations of alloxan were prepared and 5  $\mu$ l of different dilutions of the ON cell culture ( $OD_{600}$  1.0; 0.2; 0.1; 0.05; 0.02) were dropped and incubated for 5 d at 18 °C. All plates were scanned using an EPSON PERFECTION V750 PRO professional photo scanner (Epson, Hemel Hempstead, UK) and analyzed for growth inhibition by measuring the integrated intensity of the third dilution and corrected by the neighboring background.

## **Cell culture, drug treatment, immunocytochemistry and microscopy for vulvar carcinoma A431 cell line.**

For experiments, 18 mm high precision glass cover slips with a thickness of 1.5# (Paul Marienfeld GmbH & Co. KG, Lauda-Königshofen, Germany) were coated with human fibronectin (Sigma-Aldrich) at a concentration of 5  $\mu$ g cm<sup>-2</sup> for 45 min at 37 °C. In next step, the cover slips were washed one time with DMEM (Thermo Fisher Scientific, Waltham, USA) supplemented with 25 mM HEPES without phenol red (Thermo Fisher Scientific), and cells were added at a concentration of 30,000 cells cm<sup>-2</sup> in the same medium containing 2% FCS. After 2 h medium was exchanged for medium supplemented with drugs (1% (v/v) DMSO (Sigma-Aldrich), 2% FCS, 49% DMEM, 48% 1 M HEPES pH 7.5 (AppliChem, Darmstadt, Germany)) for 15 min. The final concentration of ca. 0.5 M HEPES was necessary to maintain a stable pH upon addition of alloxan up to 50 mM shortly before the experiment. Latrunculin B and cytochalasin D were solved in DMSO at a concentration of 1 mM and were stored until experiments at -20 °C. Alloxan solutions were prepared directly before experiments. After drug addition, the reactions were stopped by medium removal and immediate fixation with 4% (w/v) paraformaldehyde (Merck, Darmstadt, Germany) in PBS (pH 7.2–7.4; adjusted with NaOH at max. 60 °C)

for 15 min at room temperature. For further staining cell membranes were permeabilized for 3 min in 0.1% Triton X-100 (Sigma-Aldrich) solved in PBS (Biochrom). Alexa Fluor 546 phalloidin (Thermo Fisher Scientific) staining was performed at a concentration of 1:750 together with DAPI (Hoffmann-La Roche, Basel, Switzerland) at a concentration of 0.2  $\mu\text{g mL}^{-1}$  in PBS. Optionally in the first step cells were incubated with mouse monoclonal anti  $\alpha$ -tubulin primary antibodies DM1A (Sigma-Aldrich) for 60 min at a concentration of 1:400 and in a second step with secondary goat anti mouse antibodies coupled to Alexa Fluor 647 (Thermo Fisher Scientific) at a concentration of 1:400. Finally, cells were washed with PBS and mono-distilled  $\text{H}_2\text{O}$  before mounting with Mowiol (Carl Roth) on glass slides (76x26 mm; R. Langenbrinck, Emmendingen, Germany). Samples were dried over night at 4 °C and stored at the same temperature until microscopy within four days.

Recordings were performed at 16-bit signal resolution with a LSM 710 laser scanning confocal microscope (Zeiss, Jena, Germany; controlled by Zen black 2.1 SP3 software) equipped with an Airyscan detector and oil immersion objective 63x/1.40 DIC in super resolution mode with default pinhole settings. For detection of eGFP, an argon-ion laser (module LGK 7872 ML8) was used at 488 nm and 1% power together with a BP 420-445 + BP 465-505 filter. In case of Alexa Fluor 546, a 543 nm HeNe-laser (module LGK 7786 P) was used at 6.5% (for quantitative analysis) or 10% (supplementary figures) power together with a BP 570-620 + LP 645 filter. DAPI was recorded with a 405 nm diode laser and 0.5% power together with BP 420-480 + LP 605 filter. Alexa Fluor 647 was recorded with a 633 nm HeNe-laser (module LGK 7628-1F) and 2% power with the same filter as used for DAPI. In general, the Airyscan detector gain was set to 810 except for Alexa Fluor 647 where it was set to 760. Samples were scanned at 5.08  $\mu\text{s}$  pixel dwell time. The resolution was set to 1248 x 1248 pixel for an area of 44.1 x 44.1  $\mu\text{m}$  and z-spacing was set to 0.32  $\mu\text{m}$ .

Microscopy images were processed in Fiji distribution of ImageJ (1.51w) software package (Schindelin et al., 2012; Rueden et al., 2017). For detection of small actin particles the signal intensity of maximum grey value in every image was set to 65,534 and then the signal was filtered with unsharp mask algorithm set to sigma radius of 2.0 pixel and mask weight of 0.60. Thereafter, Yen's thresholding was applied (Yen et al.,

1995) and small particles 0.01-0.5  $\mu\text{m}^2$  with round shape (circularity 0.7-1.0) were detected using the analyze particles module. Particle brightness (integrated densitometry) was extracted from unprocessed microscopy images using the previously detected particle areas, and in next step the median particle integrated densitometry was calculated per cell with Excel 2016 (Microsoft, Redmond, USA). To compare results from images recorded at different days, the median integrated particle densitometry was divided by the average median particle densitometry of the control from the same day. For every control and drug, 20 cells were analyzed per experiment, and a total of three experiments was performed on different days. Statistics were calculated with Prism 5.01 (GraphPad, San Diego, USA) and figures were prepared with Adobe Creative Suite 6 (Adobe, San Jose, USA).

### **Statistical analysis**

Statistical analysis *via* one-way analysis of variance (ANOVA) was performed with the XL toolbox integrated into Microsoft Excel. *Post-hoc* analysis was conducted with the Bonferroni-Holm method. Student's t-test, including Welsh correction, was done using the software PRISM (GraphPad, San Diego, USA).

### **Acknowledgments**

Seeds of transgenic *Arabidopsis* reporter lines were kindly shared by Nikolaus Schlaich and Boris Voigt. We thank Prof. Wolfram Antonin and Marianna Tatarek-Nossol for providing access to the ultracentrifuge and technical assistance. We acknowledge Anja Reinstädler for excellent technical assistance.

### **Conflicts of interest**

No conflicts of interest declared.

### **Funding information**

HW was supported by a PhD fellowship from the Chinese Scholarship Council (CSC). GS is supported by the Biotechnology and Biosciences Research Council (BBSRC). Work in the laboratory of CJS on actin dynamics during the plant defense response was supported

by a grant from the US National Science Foundation (IOS-1021185).

### **Author contribution statement**

RP conceived the study; HW, WZ, MM and MS performed the experiments; HW, WZ, RP, CJS, RW and GS analyzed the data; HW and RP wrote and edited the manuscript. All authors read and approved the final version of the manuscript.

## References

- Acevedo-Garcia, J., Gruner, K., Reinstädler, A., Kemen, A., Kemen, E., Cao, L. *et al.* (2017). The powdery mildew-resistant *Arabidopsis mlo2 mlo6 mlo12* triple mutant displays altered infection phenotypes with diverse types of phytopathogens. *Sci Rep* 7:27. doi: 10.1038/s41598-017-07188-7
- Banuett, F., and Herskowitz, I. (1989). Different alleles of *Ustilago maydis* are necessary for maintenance of filamentous growth but not for meiosis. *Proc. Natl. Acad. Sci. U.S.A.* 86:5878–5882. doi: 10.1073/pnas.86.15.5878
- Bartsch, M., Gobbato, E., Bednarek, P., Debey, S., Schultze, J. L., Bautor, J. *et al.* (2006). Salicylic acid-independent ENHANCED DISEASE SUSCEPTIBILITY1 signaling in *Arabidopsis* immunity and cell death is regulated by the monooxygenase *FMO1* and the nudix hydrolase *NUDT7*. *Plant Cell* 18:1038–1051. doi: 10.1105/tpc.105.039982
- Bayles, C. J., Ghemawat, M. S., and Aist, J. R. (1990). Inhibition by 2-deoxy-D-glucose of callose formation, papilla deposition, and resistance to powdery mildew in an *mlo* barley mutant. *Physiol. Mol. Plant Pathol.* 36:63–72
- Benitez-Alfonso, Y., Cilia, M., San Roman, A., Thomas, C., Maule, A., Hearn, S. *et al.* (2009). Control of *Arabidopsis* meristem development by thioredoxin-dependent regulation of intercellular transport. *Proc. Natl. Acad. Sci. U.S.A.* 106:3615–3620. doi: 10.1073/pnas.0808717106
- Bhat, R. A., Miklis, M., Schmelzer, E., Schulze-Lefert, P., and Panstruga, R. (2005). Recruitment and interaction dynamics of plant penetration resistance components in a plasma membrane microdomain. *Proc. Natl. Acad. Sci. U.S.A.* 102:3135–3140
- Bigeard, J., Colcombet, J., and Hirt, H. (2015). Signaling mechanisms in pattern-triggered immunity (PTI). *Mol. Plant.* 8:521–539. doi: 10.1016/j.molp.2014.12.022
- Büsches, R., Hollricher, K., Panstruga, R., Simons, G., Wolter, M., Frijters, A. *et al.* (1997). The barley *Mlo* gene: A novel control element of plant pathogen resistance. *Cell* 88:695–705
- Camejo, D., Guzmán-Cedeño, Á., and Moreno, A. (2016). Reactive oxygen species, essential molecules, during plant-pathogen interactions. *Plant Physiol. Biochem.* 103:10–23. doi: 10.1016/j.plaphy.2016.02.035
- Cohen, K. L., and Bitensky, M. W. (1969). Inhibitory effects of alloxan on mammalian adenylyl cyclase. *J. Pharmacol. Exp. Ther.* 169:80–86
- Collins, N. C., Thordal-Christensen, H., Lipka, V., Bau, S., Kombrink, E., Qiu, J. L. *et al.* (2003). SNARE-protein-mediated disease resistance at the plant cell wall. *Nature* 425:973–977
- Consonni, C., Humphry, M. E., Hartmann, H. A., Livaja, M., Durner, J., Westphal, L. *et al.* (2006). Conserved requirement for a plant host cell protein in powdery mildew pathogenesis. *Nat. Genet.* 38:716–720. doi: 10.1038/ng1806
- Cooper, J. A. (1987). Effects of cytochalasin and phalloidin on actin. *J. Cell Biol.*

- Davies, K. J. (1987). Protein damage and degradation by oxygen radicals. I. general aspects. *J. Biol. Chem.* 262:9895–9901
- Davies, K. J., and Delsignore, M. E. (1987). Protein damage and degradation by oxygen radicals. III. Modification of secondary and tertiary structure. *J. Biol. Chem.* 262:9908–9913
- Davies, K. J., Delsignore, M. E., and Lin, S. W. (1987). Protein damage and degradation by oxygen radicals. II. Modification of amino acids. *J. Biol. Chem.* 262:9902–9907
- Elsner, M., Tiedge, M., Guldbakke, B., Munday, R., and Lenzen, S. (2002). Importance of the GLUT2 glucose transporter for pancreatic beta cell toxicity of alloxan. *Diabetologia* 45:1542–1549. doi: 10.1007/s00125-002-0955-x
- Freialdenhoven, A., Peterhänsel, C., Kurth, J., Kreuzaler, F., and Schulze-Lefert, P. (1996). Identification of genes required for the function of non-race-specific *mlo* resistance to powdery mildew in barley. *Plant Cell* 8:5–14
- Glawe, D. A. (2008). The powdery mildews: A review of the world's most familiar (yet poorly known) plant pathogens. *Annu. Rev. Phytopathol.* 46:27–51. doi: 10.1146/annurev.phyto.46.081407.104740
- Henty-Ridilla, J. L., Li, J., Day, B., and Staiger, C. J. (2014). ACTIN DEPOLYMERIZING FACTOR4 regulates actin dynamics during innate immune signaling in *Arabidopsis*. *Plant Cell* 26:340–352. doi: 10.1105/tpc.113.122499
- Henty-Ridilla, J. L., Shimono, M., Li, J., Chang, J. H., Day, B., Staiger, C. J. *et al.* (2013). The plant actin cytoskeleton responds to signals from microbe-associated molecular patterns. *PLoS Pathog.* 9:e1003290. doi: 10.1371/journal.ppat.1003290
- Holiday, R. (1974). “*Ustilago maydis*,” in *Handbook of Genetics Volume I*, ed. R. C. King (New York, London: Plenum Press), 575–95
- Huang, S., Blanchoin, L., Kovar, D. R., and Staiger, C. J. (2003). *Arabidopsis* capping protein (AtCP) is a heterodimer that regulates assembly at the barbed ends of actin filaments. *J. Biol. Chem.* 278:44832–44842. doi: 10.1074/jbc.M306670200
- Humphry, M., Consonni, C., and Panstruga, R. (2006). *mlo*-based powdery mildew immunity. Silver bullet or simply non-host resistance? *Mol. Plant Pathol.* 7:605–610. doi: 10.1111/j.1364-3703.2006.00362.x
- Jørgensen, J. H. (1992). Discovery, characterization and exploitation of Mlo powdery mildew resistance in barley. *Euphytica* 63:141–152
- Jørgensen, J. H. (1994). Genetics of powdery mildew resistance in barley. *Crit. Rev. Plant Sci.* 13:97–119
- Kema, G. H., and van Silfhout, C. H. (1997). Genetic variation for virulence and resistance in the wheat-*Mycosphaerella graminicola* pathosystem III. Comparative seedling and adult plant experiments 87:266–272. doi: 10.1094/PHYTO.1997.87.3.266
- Kilaru, S., Schuster, M., Latz, M., Guo, M., and Steinberg, G. (2015). Fluorescent

- markers of the endocytic pathway in *Zymoseptoria tritici*. *Fungal Genet. Biol.* 79:150–157. doi: 10.1016/j.fgb.2015.03.019
- Kilaru, S., Schuster, M., Ma, W., and Steinberg, G. (2017). Fluorescent markers of various organelles in the wheat pathogen *Zymoseptoria tritici*. *Fungal Genet. Biol.* 105:16–27. doi: 10.1016/j.fgb.2017.05.001
- Konrad, R. J., Zhang, F., Hale, J. E., Knierman, M. D., Becker, G. W., Kudlow, J. E. *et al.* (2002). Alloxan is an inhibitor of the enzyme O-linked *N*-acetylglucosamine transferase. *Biochem. Biophys. Res. Commun.* 293:207–212. doi: 10.1016/S0006-291X(02)00200-0
- Kuhn, H., Lorek, J., Kwaaitaal, M., Consonni, C., Becker, K., Micali, C. *et al.* (2017). Key components of different plant defense pathways are dispensable for powdery mildew resistance of the Arabidopsis *mlo2 mlo6 mlo12* triple mutant. *Front. Plant Sci.* 8:1006. doi: 10.3389/fpls.2017.01006
- Kusch, S., and Panstruga, R. (2017). *mlo*-based resistance: An apparently universal "weapon" to defeat powdery mildew disease. *Mol. Plant-Microbe Interact.* 30:179–189. doi: 10.1094/MPMI-12-16-0255-CR
- Kwon, C., Neu, C., Pajonk, S., Yun, H. S., Lipka, U., Humphry, M. *et al.* (2008). Co-option of a default secretory pathway for plant immune responses. *Nature* 451:835–840
- Lee, T. N., Alborn, W. E., Knierman, M. D., and Konrad, R. J. (2006). Alloxan is an inhibitor of O-GlcNAc-selective *N*-acetyl-beta-D-glucosaminidase. *Biochem. Biophys. Res. Commun.* 350:1038–1043. doi: 10.1016/j.bbrc.2006.09.155
- Lenzen, S. (2008). The mechanisms of alloxan- and streptozotocin-induced diabetes. *Diabetologia* 51:216–226. doi: 10.1007/s00125-007-0886-7
- Li, J., Cao, L., and Staiger, C. J. (2017). Capping protein modulates actin remodeling in response to reactive oxygen species during plant innate immunity. *Plant Physiol.* 173:1125–1136. doi: 10.1104/pp.16.00992
- Lipka, U., Fuchs, R., and Lipka, V. (2008). Arabidopsis non-host resistance to powdery mildews. *Curr. Opin. Plant Biol.* 11:404–411. doi: 10.1016/j.pbi.2008.04.004
- Lipka, V., Dittgen, J., Bednarek, P., Bhat, R., Wiermer, M., Stein, M. *et al.* (2005). Pre- and postinvasion defenses both contribute to nonhost resistance in *Arabidopsis*. *Science* 310:1180–1183
- Liptáková, L.'u., Bočová, B., Huttová, J., Mistrík, I., and Tamás, L. (2012). Superoxide production induced by short-term exposure of barley roots to cadmium, auxin, alloxan and sodium dodecyl sulfate. *Plant Cell Rep.* 31:2189–2197. doi: 10.1007/s00299-012-1329-6
- Ma, W., Qi, Z., Smigel, A., Walker, R. K., Verma, R., Berkowitz, G. A. *et al.* (2009). Ca<sup>2+</sup>, cAMP, and transduction of non-self perception during plant immune responses. *Proc. Natl. Acad. Sci. U.S.A.* 106:20995–21000. doi: 10.1073/pnas.0905831106
- Meglason, M. D., Burch, P. T., Berner, D. K., Najafi, H., and Matschinsky, F. M. (1986). Identification of glucokinase as an alloxan-sensitive glucose sensor of the pancreatic

beta-cell. *Diabetes* 35:1163–1173

- Miklis, M., Consonni, C., Bhat, R. A., Lipka, V., Schulze-Lefert, P., Panstruga, R. *et al.* (2007). Barley MLO modulates actin-dependent and actin-independent antifungal defense pathways at the cell periphery. *Plant Physiol.* 144:1132–1143
- Oberley, L. W. (1988). Free radicals and diabetes. *Free Radic. Biol. Med.* 5:113–124
- Peschke, E., Ebelt, H., Brömme, H. J., and Peschke, D. (2000). 'Classical' and 'new' diabetogens--comparison of their effects on isolated rat pancreatic islets in vitro. *Cell. Mol. Life Sci.* 57:158–164. doi: 10.1007/s000180050505
- Planchais, S., Glab, N., Inzé, D., and Bergounioux, C. (2000). Chemical inhibitors: A tool for plant cell cycle studies. *FEBS Lett.* 476:78–83. doi: 10.1016/S0014-5793(00)01675-6
- Qi, J., Wang, J., Gong, Z., and Zhou, J.-M. (2017). Apoplastic ROS signaling in plant immunity. *Curr. Opin. Plant Biol.* 38:92–100
- Rueden, C. T., Schindelin, J., Hiner, M. C., DeZonia, B. E., Walter, A. E., Arena, E. T. *et al.* (2017). ImageJ2: ImageJ for the next generation of scientific image data. *BMC Bioinformatics* 18:529. doi: 10.1186/s12859-017-1934-z
- Schindelin, J., Arganda-Carreras, I., Frise, E., Kaynig, V., Longair, M., Pietzsch, T. *et al.* (2012). Fiji: An open-source platform for biological-image analysis. *Nat. Methods* 9:676–682. doi: 10.1038/nmeth.2019
- Schuster, M., Kilaru, S., Ashwin, P., Lin, C., Severs, N. J., Steinberg, G. *et al.* (2011). Controlled and stochastic retention concentrates dynein at microtubule ends to keep endosomes on track. *EMBO J.* 30:652–664. doi: 10.1038/emboj.2010.360
- Schuster, M., Treitschke, S., Kilaru, S., Molloy, J., Harmer, N. J., Steinberg, G. *et al.* (2012). Myosin-5, kinesin-1 and myosin-17 cooperate in secretion of fungal chitin synthase. *EMBO J.* 31:214–227. doi: 10.1038/emboj.2011.361
- Shaw Dunn, J., and Mclellan, N.G.B. (1943). Experimental alloxan diabetes in the rat. *Lancet* 242:384–387. doi: 10.1016/S0140-6736(00)87397-3
- Theisen, U., Straube, A., and Steinberg, G. (2008). Dynamic rearrangement of nucleoporins during fungal "open" mitosis. *Mol. Biol. Cell* 19:1230–1240. doi: 10.1091/mbc.e07-02-0130
- Thordal-Christensen, H., Zhang, Z. G., Wei, Y. D., and Collinge, D. B. (1997). Subcellular localization of H<sub>2</sub>O<sub>2</sub> in plants. H<sub>2</sub>O<sub>2</sub> accumulation in papillae and hypersensitive response during the barley- powdery mildew interaction. *Plant J.* 11:1187–1194
- Torres, M. A., Jones, J. D. G., and Dangl, J. L. (2006). Reactive oxygen species signaling in response to pathogens. *Plant Physiol.* 141:373–378
- Underwood, W., and Somerville, S. C. (2013). Perception of conserved pathogen elicitors at the plasma membrane leads to relocalization of the Arabidopsis PEN3 transporter. *Proc. Natl. Acad. Sci. U.S.A.* 110:12492–12497. doi: 10.1073/pnas.1218701110



## Figure legends

**Figure 1. Alloxan partially breaks *mlo*-mediated resistance in barley.** (A) Chemical structure of alloxan and some of its analogs. (B) *Bgh* host cell entry rates on the barley *mlo-3* mutant after treatment with different concentrations of alloxan. Excised leaves of the barley *mlo-3* mutant were vacuum-infiltrated with the indicated concentrations of the chemicals. Subsequently, leaves were inoculated with *Bgh* conidiospores, and host cell entry rates were microscopically evaluated at 48 hpi. Data shown represent the mean  $\pm$  standard deviation (SD) from three independent experiments, based on four leaves for each concentration in each experiment and >100 interaction sites per leaf (i.e. >1,200 interaction sites for each concentration in total). Asterisks above columns indicate  $P < 0.05$  (one-way analysis of variance (ANOVA)) compared to the solvent control (0 mM). (C) Microscopic images of *Bgh* spores on detached leaves of a barley *mlo* mutant treated with either water (H<sub>2</sub>O) or alloxan (5 mM). app, appressorium; sh, secondary hyphae. Scale bars: 40  $\mu$ m.

**Figure 2. Alloxan suppresses *mlo*-mediated resistance and non-host resistance in *Arabidopsis*.** (A and B) Host cell entry rates of (A) *G. orontii* on the *mlo2-5 mlo6-2 mlo12-1* triple and (B) *Bgh* on *Arabidopsis* (Col-0) after treatment with different concentrations of alloxan. Data shown represent the mean  $\pm$  SD from three independent experiments, based on four leaves for each concentration in each experiment and >100 interaction sites per leaf (i.e. >1,200 interaction sites for each concentration in total). Asterisks above columns indicate  $P < 0.05$  (one-way ANOVA) compared to the solvent control (0 mM). (C and D) Representative micrographs of (C) *G. orontii* development on leaves of *Arabidopsis mlo2-5 mlo6-2 mlo12-1* triple mutant at 72 hpi and (D) of *Bgh* development on leaves of *Arabidopsis* (Col-0) at 72 hpi, either treated with water (H<sub>2</sub>O) or alloxan (10 mM). app, appressorium; sh, secondary hyphae. Scale bars: 50  $\mu$ m.

**Figure 3. Alloxan reduces callose deposition at attempted fungal penetration sites.** (A) Representative micrographs visualizing callose deposition at attempted fungal

penetration sites (indicated by arrows). Excised leaves of the barley *mlo-3* mutant were vacuum-infiltrated with either water (H<sub>2</sub>O, upper panel) or alloxan (5 mM, lower panel). Subsequently, leaves were inoculated with *Bgh* conidiospores and at 48 hpi subjected to staining with aniline blue (callose) and Commassie blue (fungal structures). Leaf samples were then observed *via* epi-fluorescence microscopy. Micrographs shown are bright field (left), epifluorescence (middle) and overlay (right). Scale bar: 20  $\mu$ m. **(B-E)** Quantification of callose deposition. Excised leaves of the barley *mlo-3* mutant **(B)**, *Arabidopsis mlo2-5 mlo6-2* double mutant **(C)**, *mlo2-5 mlo6-2 mlo12-1* triple mutant **(D)** and *Arabidopsis* wild type (Col-0) **(E)** were vacuum-infiltrated with either water (H<sub>2</sub>O) or alloxan (10 mM). Subsequently, leaves were inoculated with either *Bgh* (barley *mlo-3* and Col-0) or *G. orontii* (*mlo2-5 mlo6-2* and *mlo2-5 mlo6-2 mlo12-1*) conidiospores and at 48 hpi subjected to staining with aniline blue (callose) and Commassie blue (fungal structures). Leaf samples were then observed *via* epi-fluorescence microscopy. The percentages represent the proportion of spores with detectable callose deposits beneath attempted fungal penetration sites of leaves treated with either water (H<sub>2</sub>O) or alloxan (5 or 10 mM). Data shown represent the mean  $\pm$  SD from three independent experiments, based on four leaves in each experiment and >100 interaction sites per leaf (i.e. >1,200 interaction sites in total). Asterisks above the columns indicate  $P < 0.05$  (one-way ANOVA) compared to the water control.

**Figure 4. Alterations in organelle morphology and protein dynamics upon alloxan treatment in epidermal cells of *Arabidopsis* challenged with *Bgh*.** Excised leaves of **(A)** a transgenic *Arabidopsis* peroxisome marker line (p35S::GFP-PTS1), **(B)** a transgenic *Arabidopsis* endosome marker line (p35S::GFP-2XFYVE), **(C)** a transgenic *Arabidopsis* ER marker line (p35S::SP-GFP-HDEL) and **(D)** a transgenic *Arabidopsis* line expressing GFP-tagged PEN1/SYP121 (p35S::GFP-PEN1) were vacuum-infiltrated with either water or 10 mM alloxan. Subsequently, leaves were inoculated with *Bgh* conidiospores and viewed by CLSM at 18 hpi. Arrows indicate the attempted pathogen penetration site. Scale bars: 25  $\mu$ m. The micrographs are still images taken from Supplemental Movies S1-S4.

**Figure 5 Alloxan impairs actin filament integrity and architecture.** (A) Alloxan impairs the structure of actin filaments differently from CytE. Leaves of an actin marker line (p35S::GFP-fABD2) vacuum-infiltrated with water (upper left), alloxan (upper right) or CytE (lower left) were inoculated with *Bgh* conidiospores. Epidermal cells were viewed by confocal laser scanning microscopy (CLSM) at 18 hpi. Images shown are maximal intensity projections of z-stacks. Fungal structures were stained with propidium iodide (red). (B) Dynamics of actin filaments in epidermal cells challenged with *Bgh*. Epidermal cells of leaves of an actin marker line (p35S::GFP-fABD2) vacuum-infiltrated with either water (H<sub>2</sub>O, upper panel) or 10 mM alloxan (lower panel) were recorded by CLSM in a period of 30 min. Images shown are maximal intensity projections of z-stacks. At least five cells for each leaf and five leaves for each treatment were observed for each experiment. Three independent experiments were performed, and all experiments yielded similar results. Scale bars: 20  $\mu$ m. (C) Representative micrographs of epidermal cells from 3-d-old dark-grown hypocotyls expressing GFP-fABD2 after treatment with solvent (0.1% DMSO), 0.1, 1, 10, 100  $\mu$ M alloxan (in H<sub>2</sub>O), or 10  $\mu$ M CytD (in 0.1% DMSO) for 15 min. Images were collected by variable-angle epifluorescence microscopy (VAEM). Scale bar: 5  $\mu$ m. (D, E) Quantitative analysis of the architecture of cortical actin arrays regarding filament density (or the percentage of occupancy, (D)) and the extent of filament bundling (skewness, (E)) treated as described in (C). CytD treatment served as a positive control. Data shown represent the mean  $\pm$  SE of  $\geq$ 110 cells from ten hypocotyls per treatment. \* $P$ <0.05, \*\*\* $P$ <0.001 (Student's  $t$  test) compared to the solvent control.

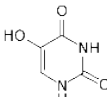
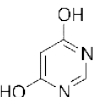
**Figure 6. Alloxan induces H<sub>2</sub>O<sub>2</sub> production in *Arabidopsis* cotyledons and rosette leaves.**

(A) Alloxan induces H<sub>2</sub>O<sub>2</sub> production in cotyledons. 7-d-old cotyledons of *Arabidopsis* (Col-0) cultured in liquid medium were incubated with either water (H<sub>2</sub>O, left) or 10 mM alloxan (right) for 3 h. Subsequently, the seedlings were stained with DAB for visualization of H<sub>2</sub>O<sub>2</sub> accumulation and representative micrographs were collected by light microscopy. Scale bars: 400  $\mu$ m. (B) Quantification of alloxan-induced H<sub>2</sub>O<sub>2</sub> accumulation in *Arabidopsis* cotyledons. Data shown represent the mean  $\pm$  SD

from three independent experiments, with ten cotyledons analyzed for each treatment and experiment. The asterisk above the column indicates  $P < 0.05$  (one-way ANOVA) compared to the water control. **(C)** Alloxan induces  $H_2O_2$  accumulation in conjunction with the disintegration of actin filaments. 7-d-old cotyledons of an *Arabidopsis* line expressing GFP-fABD2 cultured in liquid medium were incubated for 2 h with either water ( $H_2O$ , upper panel) or 10 mM alloxan (lower panel) and thereafter stained with DAB. The structure of the actin filament network and the pattern of DAB staining were observed by CLSM. Images shown for GFP are maximal intensity projections of z-stacks. BF, bright-field images. Three independent experiments were performed, and at least three cells for each seedling and three seedlings for each treatment were viewed for each experiment. Scale bars: 20  $\mu$ m. **(D)** Alloxan induces  $H_2O_2$  production in *Arabidopsis* rosette leaves. Excised rosette leaves of *Arabidopsis* (Col-0) were infiltrated with either water ( $H_2O$ ) or alloxan (10 mM) and stained with DAB at different time points after infiltration (0, 6, 12 and 24 h). Representative images were collected with a stereomicroscope with the same settings for all images. Scale bars: 2 mm. **(E)** Quantification of alloxan-induced  $H_2O_2$  accumulation in *Arabidopsis* rosette leaves. DAB staining intensity was quantified with ImageJ as described in Materials and Methods. Data shown represent the mean  $\pm$  SD of three independent experiments. Five rosette leaves for each treatment at each time point were measured for each experiment. The asterisk above the column indicates  $P < 0.05$  (one-way ANOVA) compared to the water control.

## Tables

**Table 1. List of chemicals tested in this study and their effect on *mlo*-mediated resistance in barley.**

Compound	Formula	Most effective concentration [mM] <sup>a</sup>	Host cell entry rate [%] <sup>b</sup>
Alloxan		5 mM	16
Barbituric acid		5 mM	22
Isobarbituric acid		No effect	1
4,6-dihydropyrimidine		No effect	1
Uracil		10 mM	23
2(1H)-pyrimidinone		10 mM	13
4(3H)-pyrimidinone		No effect	1
Pyrimidine		No effect	1

<sup>a</sup> Most effective concentration is the concentration at which the compound caused the highest *Bgh* entry rate.

<sup>b</sup> *Bgh* host cell entry was microscopically assessed as the proportion of germinated conidia that succeeded in the formation of micro-colonies. Host cell entry rates for solvent controls were ca. 1% for all experiments.

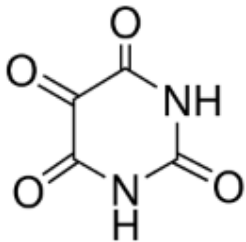
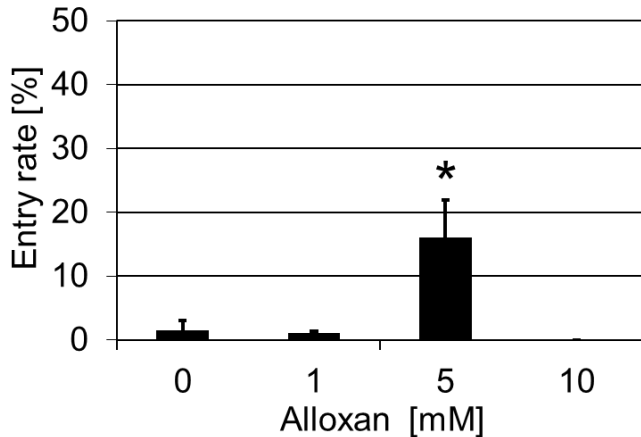
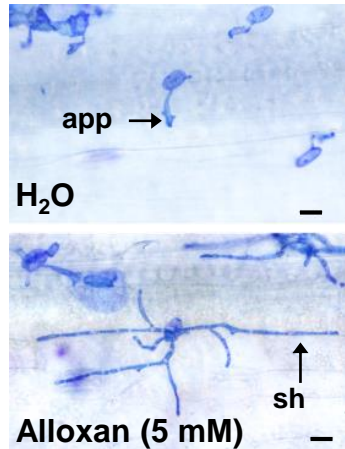
**Movie S1. Alloxan impedes the motility of peroxisomes in epidermal cells of *Arabidopsis* challenged with *Bgh*.** Excised leaves of a transgenic *Arabidopsis* peroxisome marker line (p35S::GFP-PTS1) were vacuum-infiltrated with either water (**A**) or 10 mM alloxan (**B**). Subsequently, leaves were inoculated with *Bgh* conidiospores and viewed by CLSM at 18 hpi. The videos were captured at the optimal z-position. The red circle indicates the attempted pathogen penetration site. Three independent experiments were performed, and all experiments yielded similar results. At least 3-5 cells for each leaf and five leaves for each treatment were observed for each experiment. Scale bar: 25  $\mu\text{m}$ .

**Movie S2. Alloxan impedes the motility of endosomes in epidermal cells of *Arabidopsis* challenged with *Bgh*.** Excised leaves of a transgenic *Arabidopsis* endosome marker line (p35S::GFP-2XFYVE) were vacuum-infiltrated with either water (**A**) or 10 mM alloxan (**B**). Subsequently, leaves were inoculated with *Bgh* conidiospores and viewed by CLSM at 18 hpi. The videos were captured at the optimal z-position. The red circle indicates the attempted pathogen penetration site. Three independent experiments were performed, and all experiments yielded similar results. At least 3-5 cells for each leaf and three leaves for each treatment were observed for each experiment. Scale bar: 25  $\mu\text{m}$ .

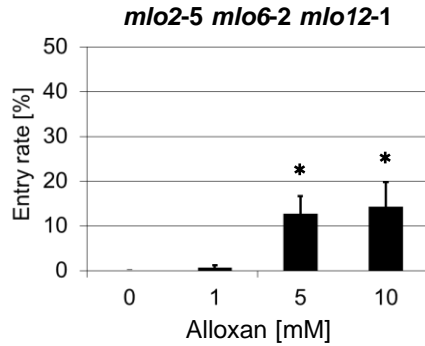
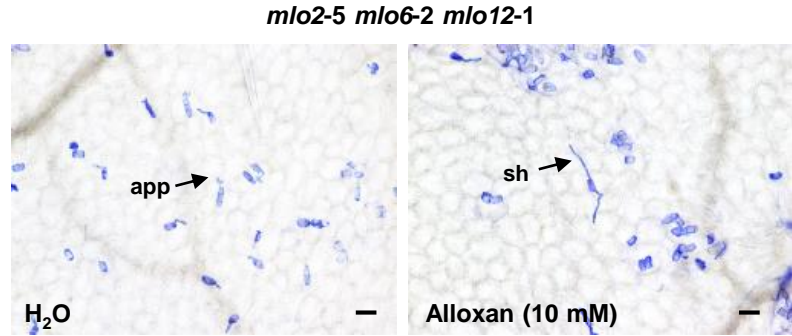
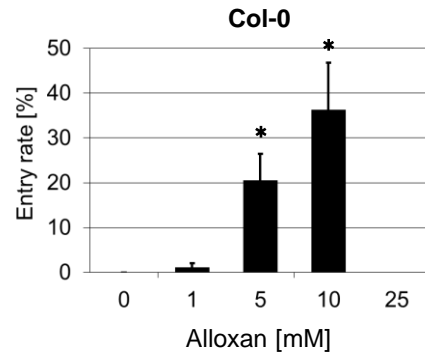
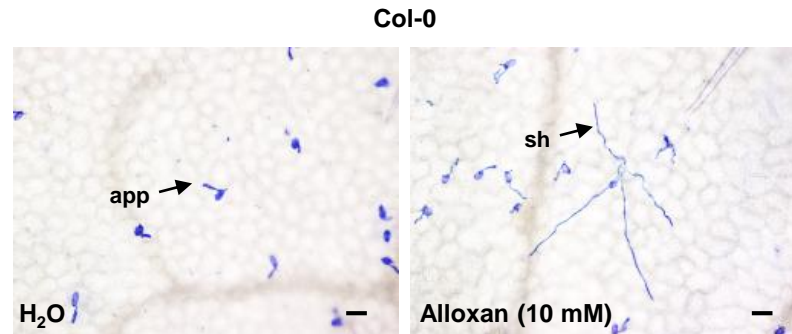
**Movie S3. Alloxan impedes the integrity and motility of the ER in epidermal cells of *Arabidopsis* challenged with *Bgh*.** Excised leaves of a transgenic *Arabidopsis* ER marker line (p35S::SP-GFP-HDEL) were vacuum-infiltrated with either water (**A**) or 10 mM alloxan (**B**). Subsequently, leaves were inoculated with *Bgh* conidiospores and viewed by CLSM at 18 hpi. The videos were captured at optimal z-position. The red circle indicates the attempted pathogen penetration site. Two independent experiments were performed, and both experiments yielded similar results. At least 3-5 cells for each leaf and three leaves for each treatment were observed for each experiment. Scale bar: 25  $\mu\text{m}$ .

**Movie S4. Alloxan affects the subcellular localization and impedes the dynamics of PEN1/SYP121 in epidermal cells of *Arabidopsis* challenged with *Bgh*.** Excised leaves of a transgenic *Arabidopsis* line expressing GFP-tagged PEN1/SYP121 (p35S::GFP-PEN1) were vacuum-infiltrated with either water (**A**) or 10 mM alloxan (**B**). Subsequently, leaves were inoculated with *Bgh* conidiospores and viewed by CLSM at 18 hpi. The videos were captured at the optimal z-position. The red circle indicates the attempted pathogen penetration site. Three independent experiments were performed, and all experiments yielded similar results. At least 3-5 cells for each leaf and three leaves for each treatment were observed for each experiment. Scale bar: 10  $\mu\text{m}$ .

**Movie S5. Effect of Alloxan on the actin cytoskeleton of *U. maydis*.** (**A**) F-actin organization in control (methanol) and alloxan-treated (1 mg/ml) yeast-like cells of *U. maydis*, visualized by a Lifeact-eGFP fusion protein. Peripheral F-actin cables connect the growing daughter cell with the mother cell. Lifeact-eGFP also labels peripheral F-actin patches that are involved in endocytosis. The 3D-reconstruction was generated from a de-convolved Z-axis image stack. Scale bar: 5  $\mu\text{m}$ . (**B**) Dynamics of F-actin patches, visualized with a fusion protein of eGFP and the F-actin-binding protein fimbrin, in control (methanol) and alloxan-treated (1 mg/ml) yeast-like *U. maydis* cells. F-actin patches are transiently visible as they get formed at sites of endocytosis. The movie represents a series of de-convolved images; time is given in the format seconds:milliseconds. Scale bar: 5  $\mu\text{m}$ .

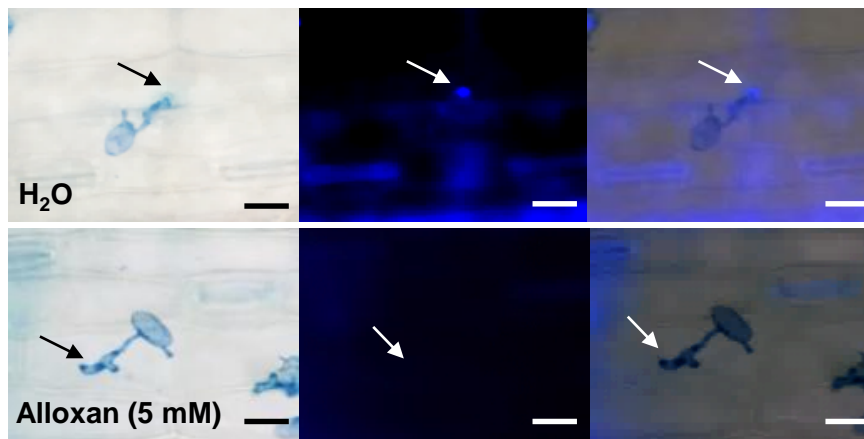
**Figure 1****A****B****C**

# Figure 2

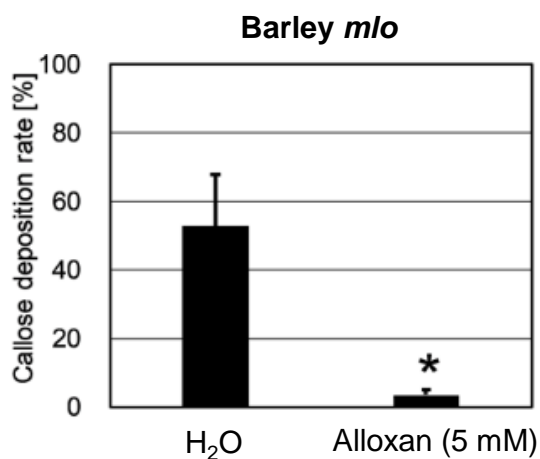
**A****C****B****D**

# Figure 3

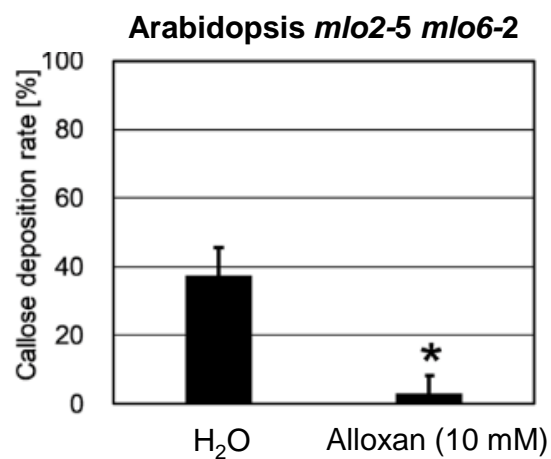
## A



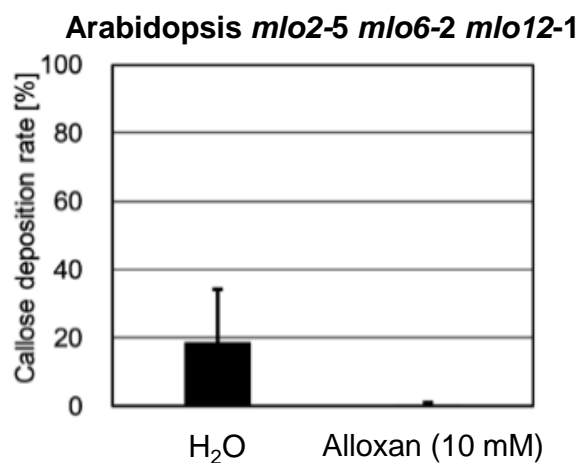
## B



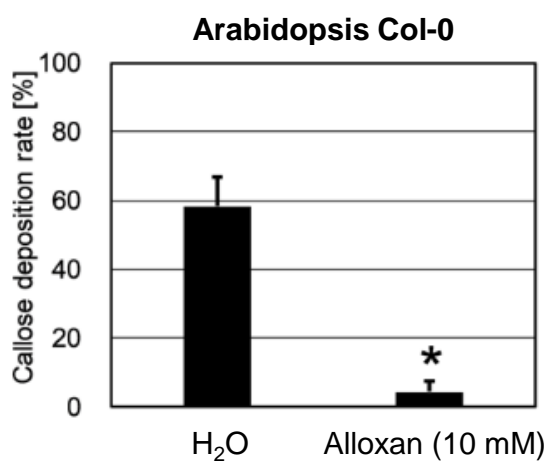
## C



## D



## E



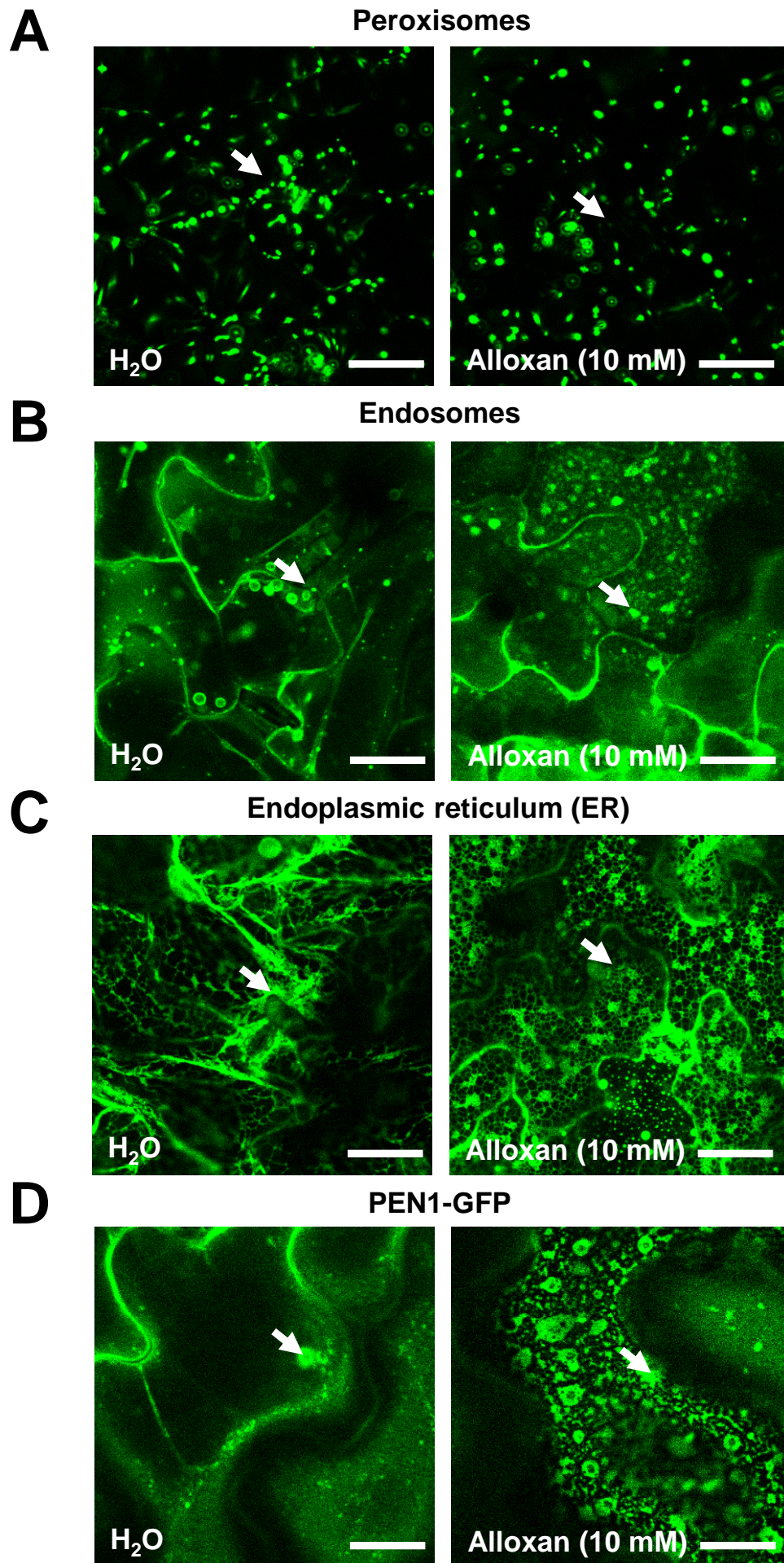


# Figure 5

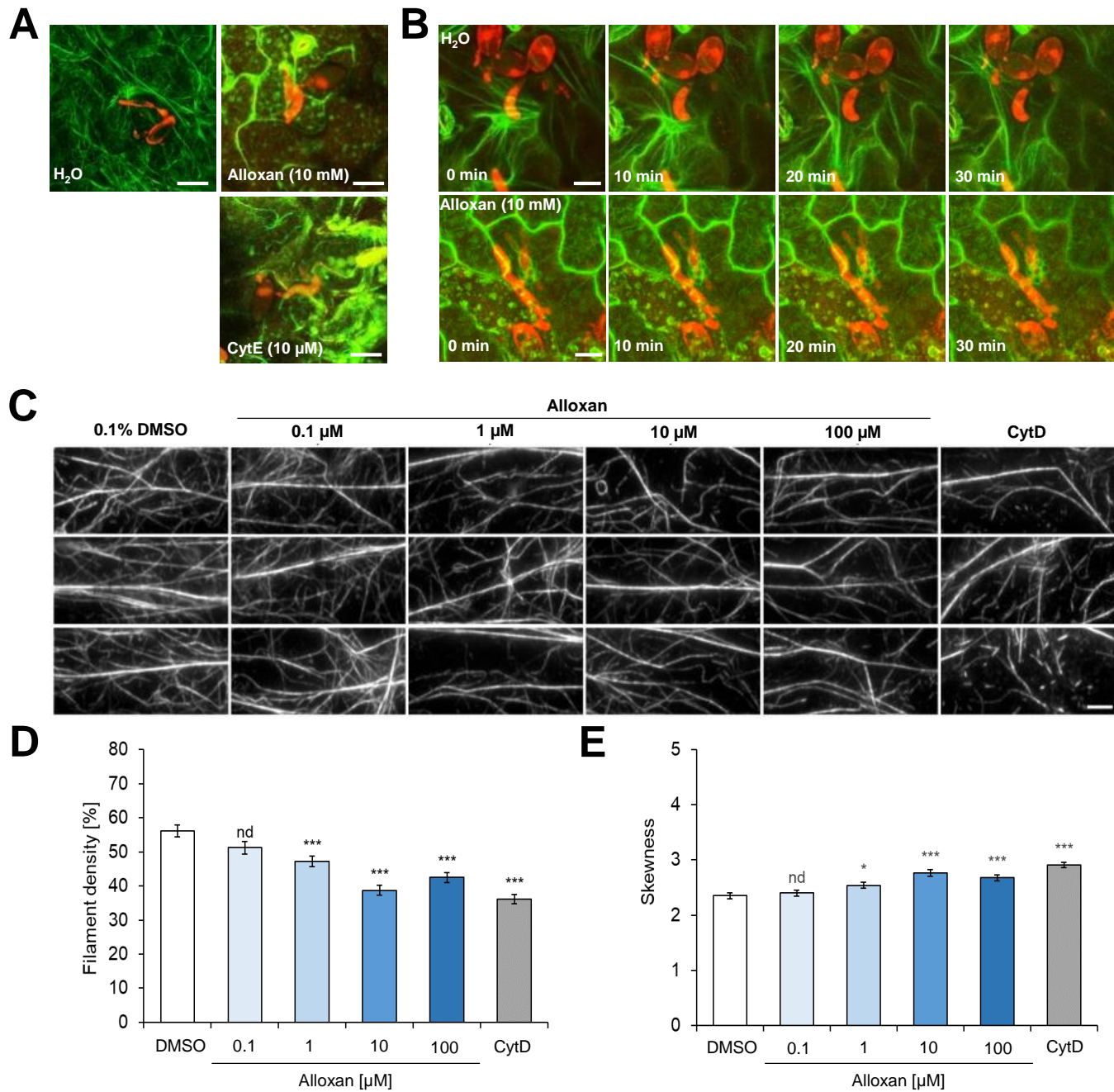


## Figure 6

